

Correlation Analyses on Binding Affinity of Sialic Acid Analogues with Influenza Virus Neuraminidase-1 Using *ab Initio* MO Calculations on Their Complex Structures

Seiji Hitaoka, Masataka Harada, Tatsusada Yoshida, and Hiroshi Chuman*

Institute of Health Biosciences, The University of Tokushima Graduate School,
1-78 Shomachi, Tokushima 770-8505, Japan

Received June 10, 2010

We carried out full *ab initio* molecular orbital calculations on complexes between neuraminidase-1 (N1-NA) in the influenza A virus and a series of eight sialic acid analogues including oseltamivir (Tamiflu) in order to quantitatively examine the binding mechanism and variation in the inhibitory potency at the atomic and electronic levels. FMO-MP2-IFIE (interfragment interaction energy at the MP2 level of *ab initio* fragment molecular orbital calculations) analyses quantitatively revealed (1) that the complex formation is driven by strong electrostatic interactions of charged functional groups in the analogues with ionized amino acid residues and water molecules in the active site of N1-NA, and (2) that the variation in the inhibitory potency among the eight analogues is determined by the dispersion and/or hydrophobic interaction energies of the 3-pentyl ether and charged amino moieties in oseltamivir with certain residues and water molecules in the active site of N1-NA. The current results will be useful for the development of new antiinfluenza drugs with high potency against various subtypes of wild-type and drug-resistant NAs.

1. INTRODUCTION

The threat of an influenza pandemic has increasingly become an issue of serious global concern. Since April (or March) 2009, a new strain of influenza A (H1N1) virus has been spreading rapidly.¹ The influenza A virus is a negative-stranded RNA virus and carries two major surface glycoproteins: hemagglutinin (HA) and neuraminidase (NA, EC 3.2.1.18) (also called sialidase), which together play critical roles in interactions with host cell surface receptors. The World Health Organization (WHO) categorizes HAs and NAs into sixteen subtypes (H1–H16) and nine subtypes (N1–N9) based on the results of antigenic and genetic analysis, respectively.² Each type of the influenza A virus is denoted by a combination of HA and NA subtypes such as H1N1 and H5N1. HAs are responsible for attaching the virus to a host cell via glycans carrying a terminal sialic acid, allowing for penetration into the host cell. After virus replication, NAs cleave the linkage formed between the HA and the sialic acid to facilitate the release and spread of the progeny virions from the infected host cell.^{3,4}

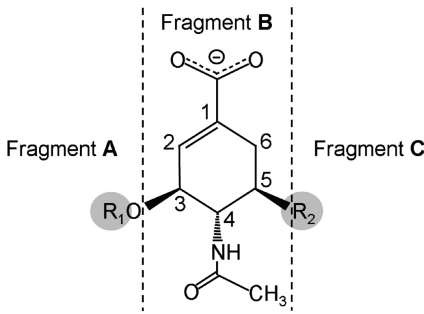
X-ray crystallographic analyses have revealed that an influenza virus NA is composed of a tetramer of four identical subunits, each composed of six four-stranded antiparallel β -sheets arranged like the blades of a propeller.^{5–7} NAs are exoglycohydrolases that hydrolyze the terminal sialic acid from glycoconjugates via a sialosyl cation transition state intermediate,^{8–10} including the viral glycoproteins themselves. Because of the essential role of NAs in the virus replication cycle, NAs have been an attractive target for antiinfluenza drugs. Several NAs exist in the influenza virus A, and they are categorized into two distinct groups according to the genetic and structural relationships between

NAs from different influenza viruses:¹¹ group-1 comprises the N1, N4, N5, and N8, and group-2 the N2, N3, N6, N7, and N9 subtypes. However, the amino acid residues in the active sites of NAs are highly conserved in the two groups. Until now, pharmaceutical companies have made efforts to develop new drugs that inhibit influenza NAs effectively. Currently available NA inhibitors, including zanamivir (Relenza)¹² and oseltamivir (Tamiflu),¹³ have been designed as transition state analogues of the sialic acids complexed with NAs. In January 2010, a new drug, peramivir (Rapiacta),¹⁴ was approved in Japan, and is expected to exhibit inhibitory activity against oseltamivir- and zanamivir-resistant viruses as well as wild-type viruses.¹⁵

To date, mutations showing a high level of resistance, especially to oseltamivir, have been widely reported.^{16–19} The His274Tyr and Asn294Ser mutations have been identified in group-1 (N1), and the Glu119Val and Arg292Lys mutations in group-2 (N2 and N9).^{20,21} These mutations have been detected in infected patients exhibiting oseltamivir resistance. Thus, the recent emergence of oseltamivir-resistant viruses indicates that the drugs currently in use may not fully protect humans and that a new generation of antiinfluenza drugs is needed.

A number of quantitative structure–activity relationship (QSAR) studies^{22–28} have been performed to elucidate the molecular mechanism of NA inhibition as well as to obtain clues for designing more potent inhibitors. However, a QSAR study alone does not provide direct information on the atomic and electronic interactions responsible for the variation in the inhibitory potency. The recent emergence of large-scale molecular calculations such as molecular orbital (MO) and molecular dynamics (MD) ones allows us to directly address the atomic and electronic interactions responsible for the NA inhibition mechanism. A number of studies involving various types of molecular calculations have also been reported:

* Corresponding author. Tel: +81-88-633-7257; fax: +81-88-633-9508; e-mail: hchuman@ph.tokushima-u.ac.jp.

Table 1. Chemical Structure and Inhibitory Potency


compound				
no.	type	R ₁ (fragment A)	R ₂ (fragment C)	pIC ₅₀ ^a
1	I	H	amino ^c	5.20
2	I	C ₃ H ₇	amino ^c	6.74
3	I	CH(Me)Et(<i>R</i>)	amino ^c	8.00
4 ^b	I	CHEt ₂	amino ^c	9.00
5	II	H	guanidino ^d	7.00
6	II	C ₃ H ₇	guanidino ^d	8.70
7	II	CH(Me)Et(<i>R</i>)	guanidino ^d	9.30
8	II	CHEt ₂	guanidino ^d	9.30

^a pIC₅₀ = -log IC₅₀ (in M). ^b Oseltamivir. ^c NH₃⁺. ^d NHC(=NH₂⁺)NH₂.

docking calculations,^{29,30} MD simulations,^{10,31–34} linear interaction energy (LIE) calculations,³⁵ comparative binding energy (COMBINE) analysis,³⁶ MM-PB(GB)/SA (molecular mechanics with Poisson–Boltzmann (generalized Born)/surface area) calculations,^{37–41} and MO calculations.⁴² Nevertheless, the atomic and electronic interactions of NAs with inhibitors are not at present fully understood quantitatively, at least.

In this work, we aimed to identify the critical interactions responsible for the variation in the inhibitory potency of a series of sialic acid analogues including oseltamivir, and to quantitatively explain the variations with the aid of molecular calculations. We constructed the structures of complexes of neuraminidase-1 (N1-NA) with eight analogues using MM/MD simulations and then carried out ab initio fragment molecular orbital (FMO) calculations on each modeled complex structure, according to our previously reported procedures.^{43–45} On the basis of the results, we quantitatively discuss the mechanism of the inhibitory interactions between N1-NA and the inhibitors at the atomic and electronic levels.

2. METHODS

2.1. Compound Set. Table 1 lists the chemical structures of the sialic acid analogues including oseltamivir (compound 4) examined in this study and their inhibitory potencies (pIC₅₀) toward the influenza A/PR/8/34 (H1N1) virus. The pIC₅₀ values were taken from the report by Kim et al.⁴⁶ The compounds listed in Table 1 are classified into type I compounds having an amino group (NH₃⁺) and type II compounds having a guanidino group (NHC(=NH₂⁺)NH₂) as substituent R₂ at the C5 position. The C3 position in types I and II compounds carries four kinds of substituents (R₁ = H, C₃H₇, CH(Me)Et(*R*), and CHEt₂): type I, (3*R*,4*R*,5*S*)-4-acetamido-5-amino-3-hydroxy-1-cyclohexene-1-carboxylic acid (compound 1) and (3*R*,4*R*,5*S*)-4-acetamido-5-amino-3-alkoxy-1-cyclohexene-1-carboxylic acids (compounds 2–4); type II, (3*R*,4*R*,5*S*)-4-acetamido-5-guanidiny-3-hydroxy-cyclohexene-

1-carboxylic acid (compound 5) and (3*R*,4*R*,5*S*)-4-acetamido-5-guanidiny-3-alkoxy-cyclohexene-1-carboxylic acids (compounds 6–8). Thus, a total of eight compounds with the common skeletal structure of 4-acetamido-cyclohex-1-ene-1-carboxylic acid were subjected to analyses. In Section 3.4, we further divide each molecular structure into three fragments: Fragments A and C contain substituents R₁ and R₂, respectively, and Fragment B is the common skeletal structure, as shown in Table 1.

2.2. Modeling of Complex Structures. The initial geometry of N1-NA complexed with oseltamivir (compound 4) was obtained from the Protein Data Bank (PDB code: 2HU4).¹¹ N1-NA in viruses exists as a tetramer, each monomer containing a functionally independent binding site and the four monomers exhibiting a nearly identical structure. Therefore, only a single monomer (chain A) was used for the modeling. N1-NA contains one calcium ion necessary for the enzymatic activity^{47–49} and structural stability.⁵⁰ Because no calcium ion or water molecules were found in 2HU4, the coordinates were taken from the structure of the complex of mutated N1-NA (His274Tyr) with oseltamivir (PDB code: 3CL0).⁵¹ The protonation state of His in the modeled complex at pH 7.0 was determined using the PDB2PQR web server,⁵² and the other ionized residues, i.e., Arg, Lys, Asp, and Glu, were treated as charged entities. One sodium ion was added as a counterion to neutralize the total -1 charge of the N1-NA–oseltamivir complex. The N1-NA–oseltamivir complex was then solvated in a truncated octahedral box of TIP3P waters extending 12 Å from the N1-NA (10153 water molecules were added in total).

MD simulations on the N1-NA–oseltamivir (compound 4) complex structure were carried out using the AMBER 10 package.⁵³ The parameters of the parm99⁵⁴ and general AMBER force field (GAFF)⁵⁵ were applied to N1-NA and oseltamivir, respectively. The partial atomic charges in oseltamivir were determined according to the RESP (restrained electrostatic potential) fitting procedure⁵⁶ with HF/6-31G* calculations (Gaussian03 program⁵⁷). It is known that the RESP-derived charge can nicely reproduce the electrostatic potential surrounding molecules.^{58–60} Before MD simulations, energy minimization with the steepest descent method, followed by the conjugate gradient method, was performed to remove ill van der Waals contacts in the initial geometry. In the first step of minimization, only hydrogen atoms were relaxed for 3000 steps, all other atoms being kept fixed, and then water molecules and the counterion were relaxed for the next 6000 steps. In the second step, all the atoms other than backbone atoms in N1-NA were optimized for 6000 steps. In the final step, the energy of the entire system was minimized for 6000 steps without any restraints.

After energy minimization, the counterion (Na⁺) and 10153 water molecules were preliminarily relaxed for 120 ps of MD, N1-NA and oseltamivir (compound 4) being kept fixed, and then the entire system was gradually heated up to 300 K over a period of 120 ps. The production MD run on the entire system was performed for 1.0 ns under the periodic boundary condition in the NPT ensemble (1.0 atm, 300 K), along with the Berendsen method,⁶¹ SHAKE algorithm,⁶² and particle–mesh–Ewald method.⁶³ The integration time step and cutoff distance of nonbonded interactions in the MD simulations were set at 1.0 fs and 10 Å, respectively.

Snapshot structures of the N1-NA–oseltamivir (compound **4**) complex were collected from the last 0.5 ns production MD trajectory at 0.1 ps intervals (5000 snapshots in total). The average MD structure was generated from the 5000 snapshot structures, and then the structure was energetically minimized. The minimized average structure of the N1-NA and oseltamivir complex was used as the initial geometry in the molecular modeling for the complex structures other than N1-NA and oseltamivir.

The initial structures of complexes of N1-NA with compounds other than compound **4** (oseltamivir) were derived from the N1-NA–compound **4** complex, which was obtained according to the aforementioned procedure. The R_1 and R_2 substituents of compounds **1–3** and **5–8** were replaced with the corresponding substituents listed in Table 1. Then, each complex structure of N1-NA with compounds **1–8** was relaxed with the steepest descent method, followed by the conjugate gradient method: only hydrogen atoms, water molecules and the counterion, and all the atoms other than backbone atoms in N1-NA were sequentially relaxed for 1000, 8000, and 8000 steps, respectively. Finally all the atoms in each complex were relaxed for 9000 steps.

Structural and thermodynamic studies^{64–66} indicated that carbohydrate-binding proteins commonly use water molecules to mediate their interactions with ligands. As shown in Figure 1, amino acid residues which are closely located in fragments **A**, **B**, and **C** of a ligand were assigned to pockets **A**, **B**, and **C**, respectively. As shown schematically in Figure 1, different numbers of tightly bound waters intervened between a ligand and NA, depending on the C5-amino (type I) and C5-guanidino (type II) groups.^{37–39} In the crystallographic structures of 23 NA–ligand complexes (PDB codes: 1BJI, 1F8C, 1F8E, 2QWD, 2QWG, 2QWH, 2QWJ, 2QWK, and 3CL0 (type I); 1L7F, 1L7G, 1L7H, 1NNC, 2CML, 2HTQ, 2QWE, 2QWF, 2QWI, 3B7E, and 3CKZ (type II)), ligands with C5-amino and C5-guanidino groups bind with two (W1 and W2 in Figure 1a) water molecules and one (W1 in Figure 1b) water molecule, respectively. The root-mean-square deviation (rmsd) values for the atomic positions of oxygen atoms in water molecules W1 and W2 in the crystallographic structures are 0.32 ($n = 23$) and 0.26 ($n = 9$) Å, respectively, indicating that their positions were nearly fixed. Accordingly, water molecules W1 and W2 for type I and W1 for type II complexes were placed in the binding site of N1-NA, and then each complex structure was further minimized.

Assuming that amino acid residues which govern interactions with ligands are mostly located in close vicinity to the active site, we prepared truncated structures of the N1-NA complexes (referred to as “truncated models”) from the full structures (“full models”) obtained through the aforementioned procedures in order to reduce the computation time for the subsequent *ab initio* MO calculations without loss of accuracy.^{67,68} The N- and C-terminal residues of fragmented peptides in the truncated structures were blocked by CH_3CO and NHCH_3 groups, respectively. The truncated model structures consist of an inhibitor (compounds **1–8**), type-specific water molecule(s), and 83 residues of N1-NA located within 8 Å from the inhibitor (residues 117–121, 133–136, 148–158, 177–180, 194–201, 221–228, 240–252, 274–278, 291–295, 300, 324–326, 346–351, 371, 405–407, 423–427, and 439). The calcium and sodium ions are ~ 10 Å apart

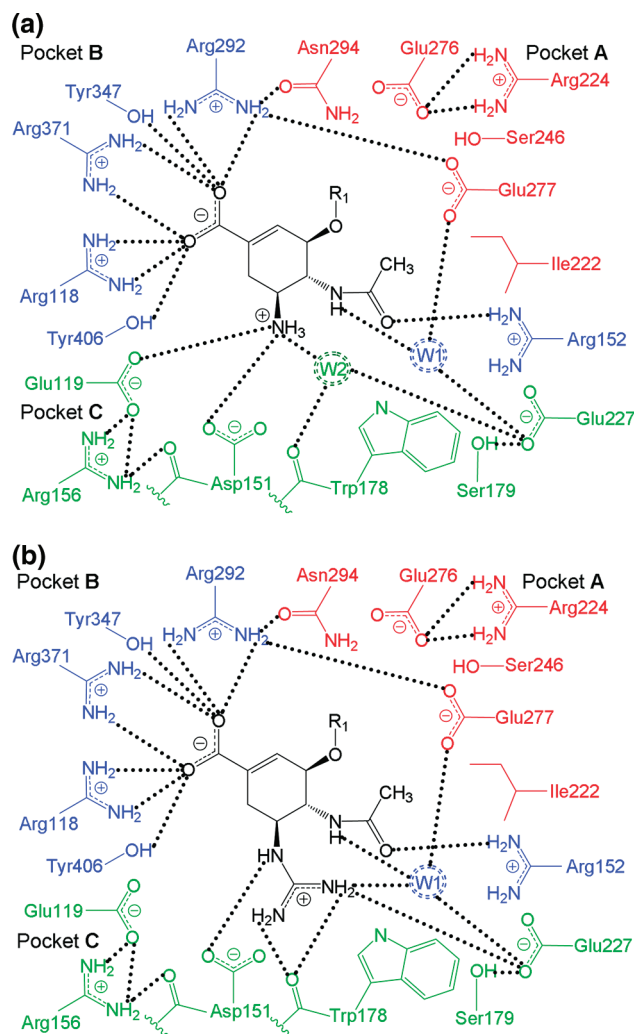


Figure 1. (a) Complexes of N1-NA with type I compounds, and (b) with type II compounds. W1 and W2 are water molecules bound in the active site. Pockets **A**, **B**, and **C** in N1-NA are colored red, blue, and green, respectively.

from the active site of N1-NA, and water molecules other than W1 and W2 are not inside the active site in the above crystallographic structures. Therefore, the complex structures without these two ions and water molecules other than W1 and W2 were used in the subsequent FMO calculations on both the full and truncated models in order to determine the interaction energy between a ligand and residues (including W1 and W2) in the active site of N1-NA.

2.3. *Ab Initio* Fragment Molecular Orbital Calculations. *Ab initio* fragment molecular orbital (FMO) calculations were performed for the eight truncated structures (compounds **1–8**) and one full model (compound **4**) structure. In the FMO algorithm, a whole molecular system is divided into a collection of small “FMO-fragments”, and the total energy of the system can be computed using the energies of FMO-fragments (monomers) and their pairs (dimers).⁶⁹ In the present study, structural units $\text{CO-NH-C}_\alpha\text{R}$ and $\text{CO-NH-C}_\alpha\text{-CH}_2\text{-S-S-CH}_2\text{-C}_\alpha$ (Cys bridge) in N1-NA were each taken as a single FMO-fragment, according to the results of our previous studies involving FMO calculations.^{43–45} As shown in Figure 2, the structures of compounds **1–8** were further divided into three FMO-fragments, **A**, **B**, and **C**, in order to discuss the contribution of each fragment to the interaction with N1-NA in Section

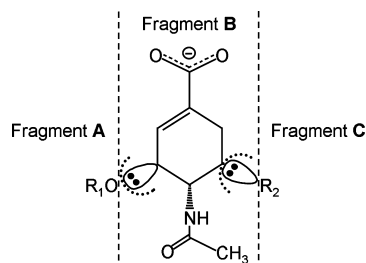


Figure 2. FMO fragmentation of compounds.

3.4.⁷⁰ Because a short-distance force was supposed to be important in the tight contact between an inhibitor and amino acid residues in the active site of N1-NA, we used MP2 level calculations to evaluate the dispersion interaction (correlation) energy between an inhibitor and N1-NA. All the FMO single-point energy calculations on the total nine complex structures were carried out at the MP2/6-31G level with the ABINIT-MP program.^{71,72} The interfragment interaction energy (IFIE) is one of the most advantageous outcomes directly obtained with the FMO procedure.⁶⁹ IFIE analyses were performed to quantitatively determine the energetic contribution of each fragment in N1-NA and a ligand to the total energy.^{43–45} In the following sections, IFIE(*i*, *j*) represents the interaction energy between the *i*- and *j*-th FMO-fragments in a ligand and N1-NA (including W1 and W2), respectively, and Σ IFIE represents the sum of the IFIE(*i*, *j*) values for all the *j*-th FMO-fragments. Σ IFIE expresses Σ IFIE(ligand, *j*), unless otherwise noted.

3. RESULTS AND DISCUSSION

3.1. N1-NA–Ligand Complex Structures. During the last 0.5 ns production MD run on the N1-NA–oseltamivir (compound **4**) complex, the average rmsd value of 385 C α atoms relative to the initial crystallographic structure (PDB code: 2HU4) was 1.11 Å. The averaged structure was generated from the MD trajectory and then minimized. The minimized structure reproduced the crystallographic structure of 2HU4 well (rmsd (385 C α atoms) = 1.17 Å). The atomic positional fluctuations of type-specific water molecules W1 and W2 during the MD simulation were 0.418 and 0.455 Å, respectively, showing that W1 and W2 remain tightly bound between oseltamivir and N1-NA. As shown in Figure 1a, W1 and W2 are located in pockets **B** and **C**, respectively, their positions being also very close to the crystallographic result. W1 forms a hydrogen-bonding network among the acetamide group of oseltamivir, Glu227, and Glu277, and W2 forms a network among the C5-amino group, Trp178, and Glu227. The above results suggest that water molecules W1 and/or W2 play critical roles in the binding between N1-NA and a ligand. The truncated model of the N1-NA–oseltamivir complex also reproduced the crystallographic structure well (rmsd (83 C α atoms) = 0.863 Å). The truncated model of the complex between N1-NA with compound **8** (type II) also well reproduced the crystallographic complex structure of N1-NA with zanamivir (PDB code: 3CKZ), which has a guanidino group (rmsd (83 C α atoms) = 0.998 Å). In type II compounds, in which the C5-amino group in type I compounds is replaced by a guanidino group, the guanidino group directly forms hydrogen bonds with Trp178 and Glu227 without the mediation of water

Table 2. $\Delta E^{\text{MP2}}_{\text{bind}}$ and Σ IFIE^{MP2} Values in the Truncated Model Structures

compound		$\Delta E^{\text{MP2}}_{\text{bind}}$ ^{a,b}	$\Delta\Delta E^{\text{MP2}}_{\text{bind}}$ ^{a,c}	Σ IFIE ^{MP2} ^a
no.	type			
1	I	−250.9	−3.6	−333.2
2	I	−252.9	−3.4	−336.0
3	I	−253.3	−2.3	−335.9
4	I	−255.5 (−259.1) ^d	−3.7	−338.0 (−340.1) ^d
5	II	−247.3		−326.6
6	II	−249.5		−332.2
7	II	−250.9		−333.4
8	II	−251.8		−333.5

^a In kcal/mol. ^b $\Delta E^{\text{MP2}}_{\text{bind}} = E(\text{complex}) - [E(\text{protein}) + E(\text{ligand})]$. ^c $\Delta\Delta E^{\text{MP2}}_{\text{bind}} = \Delta E^{\text{MP2}}_{\text{bind}}(\text{type I}) - \Delta E^{\text{MP2}}_{\text{bind}}(\text{type II})$. ^d Value within the parentheses is the energy of the full model structure of the N1-NA–oseltamivir complex.

molecules. In fact, as shown in Figure 1b, W2 was not found in the crystallographic complex structures of NA with a ligand having a guanidino group (PDB codes: 1L7F, 1L7G, 1L7H, 1NNC, 2CML, 2HTQ, 2QWE, 2QWF, 2QWI, 3B7E, and 3CKZ).

Table 2 lists the $\Delta E^{\text{MP2}}_{\text{bind}} = E(\text{complex}) - [E(\text{protein}) + E(\text{ligand})]$ and Σ IFIE^{MP2} values derived through FMO calculations on the truncated model structures of the complexes between N1-NA and compounds **1–8**, along with that on the full model structure of N1-NA–oseltamivir (compound **4**) complex. The $\Delta E^{\text{MP2}}_{\text{bind}}$ value of the truncated model structure of the N1-NA–oseltamivir complex is very close to that of the corresponding full model structure ($\Delta E^{\text{MP2}}_{\text{bind}}(\text{truncated model}) - \Delta E^{\text{MP2}}_{\text{bind}}(\text{full model}) = 3.6$ kcal/mol), clearly indicating that the binding interaction of an inhibitor with N1-NA is governed mostly by residues located close to the inhibitor. Therefore, we used the truncated model structures for the eight complexes in the FMO calculations. The difference between ΔE_{bind} and Σ IFIE in Table 2 reflects the effect of electron redistribution (relaxation).⁷³ As demonstrated in our previous studies,^{43–45} however, there is a nice linear relationship between Σ IFIE and ΔE_{bind} (in the current case, Σ IFIE^{MP2} = 1.33 $\Delta E^{\text{MP2}}_{\text{bind}}$ + 1.08, *n* = 8, *r* = 0.966), and the IFIE term for an inhibitor with each residue in a protein can provide quantitative information on the quantitative contribution of each residue to the total binding energy.

3.2. Total Interaction Energy. The total binding energies of complexes of compounds **1–8** with N1-NA are expressed by the $\Delta E^{\text{MP2}}_{\text{bind}}$ values of the eight truncated model structures. Figure 3 shows a plot between the $\Delta E^{\text{MP2}}_{\text{bind}}$ and inhibitory potency (pIC₅₀) values. The negative slope values of the two lines in Figure 3 indicate that stabilization of the binding energy increases the inhibitory potency. The pIC₅₀ values of types I and II compounds are linearly correlated with the binding energies of types I and II complexes, *r* = −0.960 and −0.962, respectively. However, the two lines have different slopes and intercepts, depending on types I and II complexes. This is probably due to differences between the amino and guanidino groups as well as those in the number of water molecules accommodated in the active site of N1-NA. In the following sections, we discuss the detailed interaction mechanism revealed by IFIE analyses.

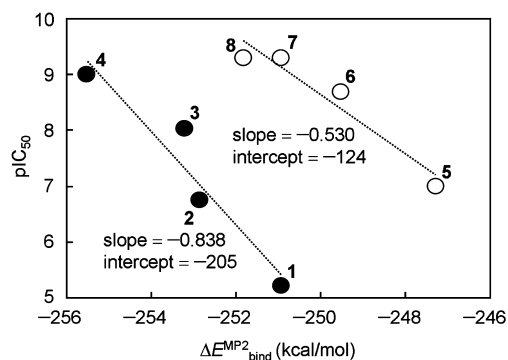


Figure 3. Plot between pIC_{50} and $\Delta E_{\text{bind}}^{\text{MP2}}$. Solid and open circles represent types I and II compounds, respectively.

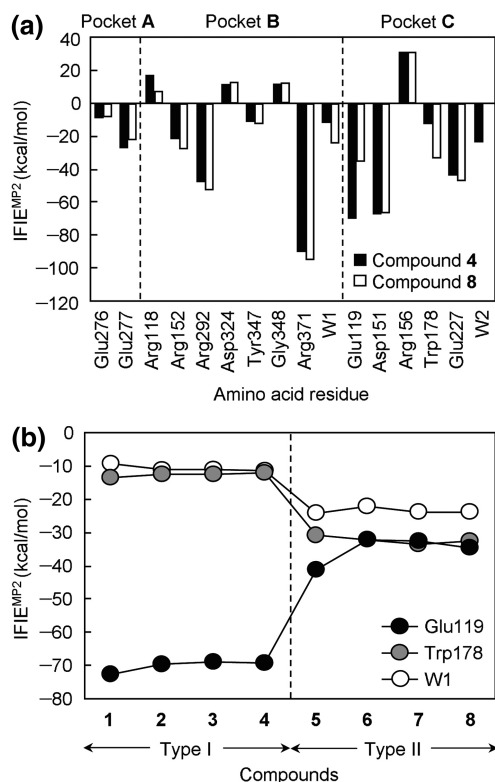


Figure 4. (a) IFIE values of compounds **4** and **8** with residues in N1-NA. (b) IFIE values of compounds **1–8** with Glu119, Trp178, and W1. Black and white bars in part a represent compounds **4** and **8**, respectively. Black, gray, and white circles in part b represent IFIE values of each compound with Glu119, Trp178, and W1 (water), respectively.

3.3. Decomposition of the Total Interaction Energy into Interaction Energies of Subsites in a Protein. Figure 4a shows the IFIE values (only shown $|IFIE| > 8.0$ kcal/mol) of amino acid residues in N1-NA with compounds **4** and **8**, which have the same substituent (3-pentyl ether) at the C3 position (fragment **A** shown in Figure 2) and exhibit the most potent inhibitory activity among the types I and II compounds, respectively. Figure 4a reveals that the total binding energy in the two compounds comes mostly from interaction energies as to residues in pockets **B** and **C**, which are both in close contact with fragment **B** (cyclohexene skeleton, an acetamide group at the C4 position, and a negatively charged carboxylate group at the C1 position) in compounds **4** and **8**. The IFIE values for FMO-fragments Arg152, Arg292, and Arg371 in pocket **B** are large negative ones (attractive interaction). As shown in Figure 1, these three

positively charged residues are involved in electrostatic and/or hydrogen-bonding interactions with fragment **B**. The acetamide and negatively charged carboxylate groups in fragment **B** are directed to pocket **B** and form hydrogen bonds with the side chain of Arg152, and with those of Arg292 and Arg371, respectively.

In addition to fragment **B**, fragment **C** (amino and guanidino groups at the C5 position for compounds **4** and **8**, respectively) significantly contributes to the total binding energy. The major stabilizing contribution from fragment **C** to the total binding energy comes from FMO-fragments Asp151 and Glu227 (pocket **C**). The amino and guanidino groups participate in the electrostatic and/or hydrogen-bonding interactions with the negatively charged side chains of Asp151 and Glu227.

The above results indicate that the tight complex formation is due to electrostatic interactions of the two compounds with ionized residues Asp151, Arg152, Glu227, Arg292, and Arg371; at the same time, the amino and guanidino groups undergo electrostatic repulsive interactions with the side chain of Arg156 in pocket **C** (30.6 and 30.0 kcal/mol, respectively).

There is a remarkable difference between type I compounds **1–4** (having an amino group) and type II compounds **5–8** (having a guanidino group) in the interactions with W1 (pocket **B**), Glu119, Trp178, and W2 (pocket **C**). Figure 4b shows significant differences in the pattern of IFIE values with W1, Glu119, and Trp178 between types I and II complexes. IFIE(type I compound, Glu119) is significantly lower than IFIE(type II compound, Glu119), while IFIE(type I compound, Trp178) and IFIE(type I compound, W1) are higher than IFIE(type II compound, Trp178) and IFIE(type II compound, W1). These differences could contribute that in the binding energy between the two types of complexes.

3.4. Interactions Which Govern Variation in the Inhibitory Potency. Next, we performed IFIE analyses involving division of the structures of compounds **1–8** into fragments **A**, **B**, and **C** (shown in Figure 2) in order to clarify the quantitative contribution of each fragment to the total binding energy. Table 3 lists $\sum IFIE^{\text{MP2}}$ (fragment **X**, N1-NA) and $\sum IFIE^{\text{corr}}$ (fragment **X**, N1-NA) for **X** = **A**, **B**, and **C**. $\sum IFIE^{\text{corr}}$ (fragment **X**, N1-NA) is defined as the energy difference between the $\sum IFIE$ values at the Møller–Plesset (MP2/6-31G) and Hartree–Fock (HF/6-31G) levels, i.e., $\sum IFIE^{\text{MP2}}$ (fragment **X**, N1-NA) – $\sum IFIE^{\text{HF}}$ (fragment **X**, N1-NA). $\sum IFIE^{\text{corr}}$ corresponds to the correlation energy term in the framework of the IFIE approximation. However, $\sum IFIE^{\text{corr}}$ (fragment **X**, N1-NA) is considered to express approximately the contribution of the dispersion (van der Waals) interaction energy to the interaction energy between fragment **X** and N1-NA.^{72,74–76}

As shown in Table 3, the contribution of the sum of $\langle \sum IFIE^{\text{MP2}}$ (fragment **B**, N1-NA) and $\langle \sum IFIE^{\text{MP2}}$ (fragment **C**, N1-NA) reaches 95% of the total binding energy, where $\langle \rangle$ denotes the average. The dispersion interaction energies $\langle \sum IFIE^{\text{corr}}$ (fragment **B**, N1-NA) and $\langle \sum IFIE^{\text{corr}}$ (fragment **C**, N1-NA) are 22 and 7% of $\langle \sum IFIE^{\text{MP2}}$ (fragment **B**, N1-NA) and $\langle \sum IFIE^{\text{MP2}}$ (fragment **C**, N1-NA), respectively, indicating that the total binding energy comes mostly from the electrostatic interactions, as mentioned in the previous section. To summarize these results, the complex formation is governed by the strong electrostatic interactions among

Table 3. $\Sigma\text{IFIE}^{\text{MP2}}$ and $\Sigma\text{IFIE}^{\text{corr}}$ Values^a

compound		ΣIFIE (fragment A, N1-NA)			ΣIFIE (fragment B, N1-NA)		ΣIFIE (fragment C, N1-NA)	
no.	type	pIC ₅₀	MP2	corr ^b	MP2	corr ^b	MP2	corr ^b
1	I	5.20	-13.3	0.3	-158.7	-34.9	-161.7	-7.4
2	I	6.74	-19.0	-7.6	-156.7	-36.4	-158.1	-7.1
3	I	8.00	-20.4	-9.3	-157.3	-37.5	-156.5	-7.2
4	I	9.00	-21.4	-12.9	-157.9	-37.4	-156.4	-7.1
variance ^c	I		9.8	23.5	0.5	1.1	4.5	0.0
5	II	7.00	-13.9	0.3	-154.7	-32.8	-154.5	-14.5
6	II	8.70	-17.1	-7.9	-155.9	-33.5	-154.2	-13.7
7	II	9.30	-18.7	-10.5	-156.0	-33.9	-153.0	-13.9
8	II	9.30	-19.1	-13.2	-156.2	-33.6	-152.3	-13.7
variance ^c	II		4.1	25.6	0.3	0.1	0.8	0.1
average	I + II		-17.9	-7.6	-156.7	-35.0	-155.8	-10.6
contribution ^d (%)	I + II		5.4		47.4		47.2	
variance ^c	I + II		7.4	24.6	1.4	3.0	8.1	11.5

^a In kcal/mol. ^b MP2 correlation energy contribution ($\Sigma\text{IFIE}^{\text{MP2}}$ (fragment X, N1-NA) - $\Sigma\text{IFIE}^{\text{HF}}$ (fragment X, N1-NA), for X = A, B, and C). ^c In kcal²/mol². ^d $\langle \Sigma\text{IFIE}^{\text{MP2}}$ (fragment X, N1-NA) \rangle divided by summation of $\langle \Sigma\text{IFIE}^{\text{MP2}}$ (fragment Y, N1-NA) \rangle for Y = A, B, and C, where $\langle \rangle$ denotes the average.

fragments B, C, and the ionized amino acid residues, as shown in the previous section.

The contribution of fragment B to the variance in the binding energy was not expected to be significant, because fragment B is the common skeleton of compounds 1–8. In fact, the variance in $\Sigma\text{IFIE}^{\text{MP2}}$ (fragment B, N1-NA) (denoted as var.[ΣIFIE] hereafter) for types I and II complexes ($n = 8$) has the smallest value among those for fragments A, B, and C with N1-NA. Var.[$\Sigma\text{IFIE}^{\text{MP2}}$ (fragment B, N1-NA)] and var.[$\Sigma\text{IFIE}^{\text{corr}}$ (fragment B, N1-NA)] for types I and II complexes are somewhat large but still much smaller than the corresponding ones for fragments A and C. This is possibly due to subtle differences in the contact distances of the skeleton from residues in pocket B between the two types. Despite the great stabilization of the total binding energy derived from fragment B, fragment B does not make a significant contribution to the variance in total binding energy.

Var.[$\Sigma\text{IFIE}^{\text{MP2}}$ (fragment C, N1-NA)] (8.1 kcal²/mol²) is slightly larger than var.[$\Sigma\text{IFIE}^{\text{MP2}}$ (fragment A, N1-NA)] (7.4 kcal²/mol²) for types I and II complexes. However, it should be noted that the large var.[$\Sigma\text{IFIE}^{\text{MP2}}$ (fragment C, N1-NA)] value is due to differences between the two types of complexes but not from those within the same type of complex. This is confirmed by (1) for type I complexes; var.[$\Sigma\text{IFIE}^{\text{MP2}}$ (fragment C, N1-NA)] (4.5 kcal²/mol²) < var.[$\Sigma\text{IFIE}^{\text{MP2}}$ (fragment A, N1-NA)] (9.8 kcal²/mol²), and (2) for type II complexes; var.[$\Sigma\text{IFIE}^{\text{MP2}}$ (fragment C, N1-NA)] (0.8 kcal²/mol²) < var.[$\Sigma\text{IFIE}^{\text{MP2}}$ (fragment A, N1-NA)] (4.1 kcal²/mol²).

Var.[$\Sigma\text{IFIE}^{\text{corr}}$ (fragment C, N1-NA)] for type I complexes and var.[$\Sigma\text{IFIE}^{\text{corr}}$ (fragment C, N1-NA)] for type II complexes are both negligible. However, var.[$\Sigma\text{IFIE}^{\text{corr}}$ (fragment C, N1-NA)] for types I and II complexes is considerably large (11.5 kcal²/mol²). This finding reflects the significant difference in the type-dependent dispersion interaction energy for fragment C with certain residues in pocket C between types I and II complexes; the average differences (type I – type II) in the dispersion interaction energy for fragment C with Trp178 and that with Asp151 are 3.2 and 1.5 kcal/mol, respectively. This difference in the ΣIFIE values of fragment C with residues in pocket C between the two types of

complexes is probably one of the reasons for why the plot between pIC₅₀ and $\Delta E^{\text{MP2}}_{\text{bind}}$ shown in Figure 3 separates into the two different lines, depending on the type.

The $\langle \Sigma\text{IFIE}^{\text{MP2}}$ (fragment A, N1-NA) \rangle value is about 10% of fragments B and C. Unlike in the case of fragments B and C, the large ratio between $\Sigma\text{IFIE}^{\text{corr}}$ (fragment A, N1-NA) and $\Sigma\text{IFIE}^{\text{MP2}}$ (fragment A, N1-NA) indicates that the dispersion interactions arising from fragment A, instead of electrostatic interactions, make a dominant contribution to the binding energy between fragment A and N1-NA. This is probably because fragment A (OR₁, R₁ = H and alkyl) has a less polar group than the charged carboxylate, amino, and guanidino groups in fragments B and C. As can be seen in Table 3, each of the following three var.[$\Sigma\text{IFIE}^{\text{corr}}$ (fragment A, N1-NA)] values is the largest value among those of fragments A, B, and C: (1) var.[$\Sigma\text{IFIE}^{\text{corr}}$ (fragment A, N1-NA)] for type I complexes ($n = 4$), (2) for type II complexes ($n = 4$), and (3) for types I and II complexes ($n = 8$). These large values of variance suggest that the dispersion interactions of fragment A with N1-NA determine most of the variance in the total binding energy.

The results described above lead to the following important conclusions: (1) the variation in the inhibitory potency pIC₅₀ values, regardless of the differences in the two types of complexes, is determined by that in the dispersion interaction energy, and (2) the dispersion interaction energy is mostly due to fragment A and partially fragment C. Figure 5 shows a plot between pIC₅₀ and $\Sigma\text{IFIE}^{\text{corr}}$ (fragments A and C, N1-NA) (pIC₅₀ = -0.223 $\Sigma\text{IFIE}^{\text{corr}}$ + 3.85, $n = 8$ (types I and II complexes), $r = -0.961$).

Figure 6a shows IFIE^{corr} values for the 3-pentyl ether (R₁ = CH₂Et₂) group in compound 4 (oseltamivir) and amino acid residues, which are in close contact with this group. Figure 6b shows a three-dimensional view of the 3-pentyl ether group surrounded by the residues shown in Figure 6a, Ile222, Arg224, Ser246, Glu276, Glu277, Arg292, and Asn294. These seven residues except Arg292 are in pocket A, as shown in Figure 1a. The hydrogen-bond formation between the side chains of Arg224 and Glu276 has been considered to be important in creating pocket A with an optimum shape and size for accommodating the 3-pentyl ether group of oseltamivir into this pocket.^{16,77,78}

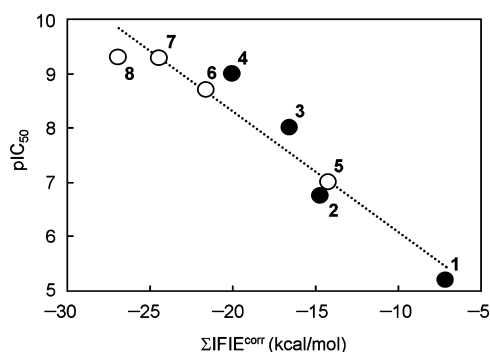


Figure 5. Plot between pIC_{50} and $\Sigma IFIE^{corr}$ (fragments **A** and **C**, N1-NA). Solid and open circles represent types I and II compounds, respectively.

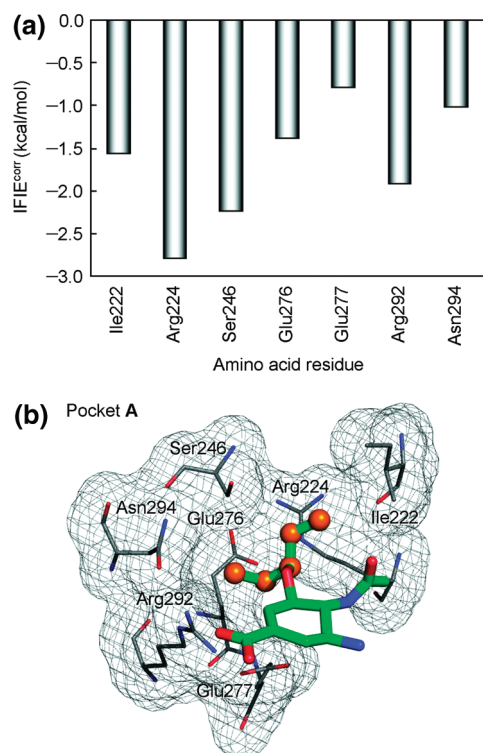


Figure 6. (a) Dispersion interaction energies of amino acid residues in pocket **A** with fragment **A** in compound **4** (oseltamivir). (b) View of compound **4** (ball and stick model) accommodated in pocket **A** (gray).

The water-accessible surface area (ASA)⁷⁹ has often been used as an effective parameter to represent the hydrophobic interaction energy quantitatively.^{80,81} ΔASA is defined as $ASA(\text{complex}) - ASA(\text{protein}) - ASA(\text{inhibitor})$. The ΔASA value only for the above seven residues correlates well with the sum of the $IFIE^{corr}$ values of fragment **A** with the seven residues ($n = 8$, $r = 0.946$), indicating that the interaction of fragment **A** could be due to the hydrophobic and/or the dispersion interactions. A significant correlation was also found between the ΔASA value and the inhibitory potency pIC_{50} ($n = 8$, $r = -0.892$).

The overall free-energy change $\Delta G = -2.303 RT pIC_{50}$ during typical ligand–protein complex formation includes other energy terms such as the solvation free-energy, conformational entropy, and deformation energy, as well as the total binding enthalpy (ΔE^{MP2}_{bind}) terms.⁴⁵ The dispersion and hydrophobic interaction energies arising from fragment **A** can be expected to be linear with pIC_{50} , assuming that

$|\Delta \Delta G^0_{bind}|$ is considerably smaller than $|\Delta \Delta E^{MP2}_{bind}|$ ($|\langle \Delta \Delta E^{MP2}_{bind} \rangle| = 3.3$ kcal/mol, as seen in Table 2) for each pair of compounds having the same substituent (OR_i) in fragment **A** in types I and type II compounds (total of four pairs). In the above $\Delta \Delta G^0_{bind} = \Delta G^0_{bind}(\text{type I}) - \Delta G^0_{bind}(\text{type II})$ represents the sum of free-energy differences in various free-energy terms other than those correlated with the dispersion and hydrophobic interaction energy terms. One of the most possible reasons for the inequality $|\Delta \Delta G^0_{bind}| < |\Delta \Delta E^{MP2}_{bind}|$ could be due to the enthalpy–entropy compensation:⁸² the energy difference in the entropic term ($-T\Delta S$) such as the conformational entropy⁸³ counteracts that in the enthalpic term (ΔE^{MP2}_{bind}). Recently Gloster et al. demonstrated the enthalpy–entropy compensation for the inhibition of β -glucosidase,^{84,85} although neuraminidases are classified into a different family of glycosidases. They showed a significant correlation between ΔH and $-T\Delta S$ ($r = -0.91$ and slope = -0.90) in the binding of 18 transition state analogue inhibitors with β -glucosidase, using the isothermal titration calorimetry data.

The dispersion and hydrophobic interaction energy terms, along with those correlated with these terms, contribute to the total binding free-energy independently of the rest of free-energy terms, because these interactions are considered to be “local interactions”, which only occur effectively between parts that are located close to each other, fragment **A**, and the seven residues. In the above case, regardless of the differences in the two types of complexes, pIC_{50} exhibits a significant correlation with the dispersion and hydrophobic interaction energies.

4. CONCLUSIONS

We carried out ab initio FMO calculations on model structures of complexes between N1-NA and eight sialic acid analogues (compounds **1–8**) including oseltamivir in order to quantitatively elucidate the inhibitory interaction mechanism at the atomic and electronic levels.

The total binding energy comes mostly from electrostatic interactions of charged functional groups in fragments **B** and **C** of compounds **1–8** with ionized amino acid residues in pockets **B** and **C** of N1-NA. Because of the tight electrostatic complex formation, where short-distance interactions such as the dispersion interaction become particularly important, we carried out MP2 level ab initio MO calculations.

The FMO-MP2-IFIE analyses revealed (1) significant differences in the pattern of electrostatic interaction energies of fragment **C** (amino and guanidino groups in types I and II compounds, respectively) with ionized residues and water molecules in pocket **C**, between types I and II complexes, and (2) regardless of differences in the two types, the inhibitory potency, pIC_{50} , of all the eight compounds is well linear with the dispersion and hydrophobic interaction energies between fragment **A** and residues mostly in pocket **A**.

We reemphasize that the structural factors that stabilize the total binding free-energy are sometimes different from those that govern the variation in the total binding free-energy among a series of ligands.

The findings in this study provide detailed information on the oseltamivir-resistance caused by the Glu119Val, His274Tyr, and Asn294Ser mutations. The Glu119Val mutation induces

resistance to oseltamivir (having an amino group) but not to zanamivir (having a guanidino group). This difference in sensitivity corresponds well to the finding that the amino group interacts with Glu119 more strongly than the guanidino group. The His274Tyr and Asn294Ser mutations detected in N1-NA also confer oseltamivir-resistance. The His274Tyr and Asn294Ser mutations change the shape of pocket A entirely, supporting the importance of the shape-specific interaction between the 3-pentyl ether group in oseltamivir and residues in pocket A.⁵¹

Currently available drugs oseltamivir, zanamivir, and peramivir are sophisticatedly designed so as to position their fragments A, B, and C in pockets A, B, and C in N1-NA, respectively. The possibility of further structural modifications is suggested by the finding that the amino and guanidino groups (fragment C) are forced to undergo an unfavorable interaction with the side chain of Arg156. In fact, attempts to modify the amino and guanidino groups in fragment C have been made to form a new hydrogen-bond with Arg156.^{30,41,86}

The current results will be a useful guide for the development of new antiinfluenza drugs with high potency against various subtypes of wild-type and drug-resistant NAs, as well as with high bioavailability. The present study shows that the current approach is able to describe the quantitative free-energy profile of complex formation of N1-NA with the eight sialic acid analogues. The approach is based upon the portioning of the total free-energy change into additive contributions from different structural fragments in the complex⁸⁷ and also into those from various free-energy terms.^{88,89} Bren et al.^{90,91} theoretically demonstrated that the additivity can be justified as the first-order approximation. The accuracy of approximation is expected to be good especially for the LFEP (linear free-energy principle) congeneric series.⁴⁵ Such approaches using the additivity and LFEP give valuable information to understand the ligand–receptor interaction mechanism at the atomic and electronic levels and to assist the lead optimization process for developing new drugs.

ACKNOWLEDGMENT

This work was supported by the Japan Science and Technology Corp. (JST-CREST) and Grants-in-Aid for Scientific Research (No. 20590036) from the Ministry of Education, Culture, Sports, Science and Technology.

REFERENCES AND NOTES

- (1) Centers for Disease Control and Prevention. Update: novel influenza A (H1N1) virus infections — worldwide. May 6, 2009. *Morb. Mortal. Wkly. Rep.* **2009**, 58, 453–458.
- (2) World Health Organization. A revision of the system of nomenclature for influenza viruses: a WHO memorandum. *Bull. World Health Organ.* **1980**, 58, 585–591.
- (3) De Clercq, E. Antiviral agents active against influenza A viruses. *Nat. Rev. Drug Discovery* **2006**, 5, 1015–1025.
- (4) von Itzstein, M. The war against influenza: discovery and development of sialidase inhibitors. *Nat. Rev. Drug Discovery* **2007**, 6, 967–974.
- (5) Varghese, J. N.; Colman, P. M. Three-dimensional structure of the neuraminidase of influenza virus A/Tokyo/3/67 at 2.2 Å resolution. *J. Mol. Biol.* **1991**, 221, 473–486.
- (6) Varghese, J. N.; Laver, W. G.; Colman, P. M. Structure of the influenza virus glycoprotein antigen neuraminidase at 2.9 Å resolution. *Nature* **1983**, 303, 35–40.
- (7) Colman, P. M.; Varghese, J. N.; Laver, W. G. Structure of the catalytic and antigenic sites in influenza virus neuraminidase. *Nature* **1983**, 303, 41–44.
- (8) Chong, A. K. J.; Pegg, M. S.; von Itzstein, M. Characterisation of an ionisable group involved in binding and catalysis by sialidase from influenza virus. *Biochem. Int.* **1991**, 24, 165–171.
- (9) Chong, A. K. J.; Pegg, M. S.; Taylor, N. R.; von Itzstein, M. Evidence for a sialosyl cation transition-state complex in the reaction of sialidase from influenza virus. *Eur. J. Biochem.* **1992**, 207, 335–343.
- (10) Taylor, N. R.; von Itzstein, M. Molecular modeling studies on ligand binding to sialidase from influenza virus and the mechanism of catalysis. *J. Med. Chem.* **1994**, 37, 616–624.
- (11) Russell, R. J.; Haire, L. F.; Stevens, D. J.; Collins, P. J.; Lin, Y. P.; Blackburn, G. M.; Hay, A. J.; Gamblin, S. J.; Skehel, J. J. The structure of H5N1 avian influenza neuraminidase suggests new opportunities for drug design. *Nature* **2006**, 443, 45–49.
- (12) von Itzstein, M.; Wu, W.-Y.; Kok, G. B.; Pegg, M. S.; Dyason, J. C.; Jin, B.; Phan, T. V.; Smythe, M. L.; White, H. F.; Oliver, S. W.; Colman, P. M.; Varghese, J. N.; Ryan, D. M.; Woods, J. M.; Bethell, R. C.; Hotham, V. J.; Cameron, J. M.; Penn, C. R. Rational design of potent sialidase-based inhibitors of influenza virus replication. *Nature* **1993**, 363, 418–423.
- (13) Kim, C. U.; Lew, W.; Williams, M. A.; Liu, H.; Zhang, L.; Swaminathan, S.; Bischofberger, N.; Chen, M. S.; Mendel, D. B.; Tai, C. Y.; Laver, W. G.; Stevens, R. C. Influenza neuraminidase inhibitors possessing a novel hydrophobic interaction in the enzyme active site: design, synthesis, and structural analysis of carbocyclic sialic acid analogues with potent anti-influenza activity. *J. Am. Chem. Soc.* **1997**, 119, 681–690.
- (14) Babu, Y. S.; Chand, P.; Bantia, S.; Kotian, P.; Dehghani, A.; El-Kattan, Y.; Lin, T.-H.; Hutchison, T. L.; Elliott, A. J.; Parker, C. D.; Ananth, S. L.; Horn, L. L.; Laver, G. W.; Montgomery, J. A. BCX-1812 (RWJ-270201): discovery of a novel, highly potent, orally active, and selective influenza neuraminidase inhibitor through structure-based drug design. *J. Med. Chem.* **2000**, 43, 3482–3486.
- (15) Gubareva, L. V.; Webster, R. G.; Hayden, F. G. Comparison of the activities of zanamivir, oseltamivir, and RWJ-270201 against clinical isolates of influenza virus and neuraminidase inhibitor-resistant variants. *Antimicrob. Agents Chemother.* **2001**, 45, 3403–3408.
- (16) Moscona, A. Oseltamivir resistance—disabling our influenza defenses. *N. Engl. J. Med.* **2005**, 353, 2633–2636.
- (17) Reece, P. A. Neuraminidase inhibitor resistance in influenza viruses. *J. Med. Virol.* **2007**, 79, 1577–1586.
- (18) McKimm-Breschkin, J. L.; Selleck, P. W.; Usman, T. B.; Johnson, M. A. Reduced sensitivity of influenza A (H5N1) to oseltamivir. *Emerging Infect. Dis.* **2007**, 13, 1354–1357.
- (19) Richard, M.; Deléage, C.; Barthélémy, M.; Lin, Y. P.; Hay, A.; Lina, B.; Ferraris, O. Impact of influenza A virus neuraminidase mutations on the stability, activity, and sensibility of the neuraminidase to neuraminidase inhibitors. *J. Clin. Virol.* **2008**, 41, 20–24.
- (20) Ferraris, O.; Lina, B. Mutations of neuraminidase implicated in neuraminidase inhibitors resistance. *J. Clin. Virol.* **2008**, 41, 13–19.
- (21) Collins, P. J.; Haire, L. F.; Lin, Y. P.; Liu, J.; Russell, R. J.; Walker, P. A.; Martin, S. R.; Daniels, R. S.; Gregory, V.; Skehel, J. J.; Gamblin, S. J.; Hay, A. J. Structural basis for oseltamivir resistance of influenza viruses. *Vaccine* **2009**, 27, 6317–6323.
- (22) Verma, R. P.; Hansch, C. A QSAR study on influenza neuraminidase inhibitors. *Bioorg. Med. Chem.* **2006**, 14, 982–996.
- (23) Zhang, J.; Yu, K.; Zhu, W.; Jiang, H. Neuraminidase pharmacophore model derived from diverse classes of inhibitors. *Bioorg. Med. Chem. Lett.* **2006**, 16, 3009–3014.
- (24) Zheng, M.; Yu, K.; Liu, H.; Luo, X.; Chen, K.; Zhu, W.; Jiang, H. QSAR analyses on avian influenza virus neuraminidase inhibitors using CoMFA, CoMSIA, and HQSAR. *J. Comput.-Aided Mol. Des.* **2006**, 20, 549–566.
- (25) Du, Q.-S.; Huang, R.-B.; Wei, Y.-T.; Du, L.-Q.; Chou, K.-C. Multiple field three dimensional quantitative structure-activity relationship (MF-3D-QSAR). *J. Comput. Chem.* **2008**, 29, 211–219.
- (26) Abu Hamad, A. M.; Taha, M. O. Pharmacophore modeling, quantitative structure-activity relationship analysis, and shape-complemented in silico screening allow access to novel influenza neuraminidase inhibitors. *J. Chem. Inf. Model.* **2009**, 49, 978–996.
- (27) Du, Q.-S.; Huang, R.-B.; Wei, Y.-T.; Pang, Z.-W.; Du, L.-Q.; Chou, K.-C. Fragment-based quantitative structure-activity relationship (FB-QSAR) for fragment-based drug design. *J. Comput. Chem.* **2009**, 30, 295–304.
- (28) Sun, J.; Cai, S.; Yan, N.; Mei, H. Docking and 3D-QSAR studies of influenza neuraminidase inhibitors using three-dimensional holographic vector of atomic interaction field analysis. *Eur. J. Med. Chem.* **2010**, 45, 1008–1014.
- (29) Du, Q.-S.; Wang, S.-Q.; Chou, K.-C. Analogue inhibitors by modifying oseltamivir based on the crystal neuraminidase structure for treating

- drug-resistant H5N1 virus. *Biochem. Biophys. Res. Commun.* **2007**, *362*, 525–531.
- (30) Mitrasinovic, P. M. On the structure-based design of novel inhibitors of H5N1 influenza A virus neuraminidase (NA). *Biophys. Chem.* **2009**, *140*, 35–38.
- (31) Taylor, N. R.; von Itzstein, M. A structural and energetics analysis of the binding of a series of *N*-acetylneuraminic-acid-based inhibitors to influenza virus sialidase. *J. Comput.-Aided Mol. Des.* **1996**, *10*, 233–246.
- (32) Amaro, R. E.; Cheng, X.; Ivanov, I.; Xu, D.; McCammon, J. A. Characterizing loop dynamics and ligand recognition in human- and avian-type influenza neuraminidases via generalized born molecular dynamics and end-point free energy calculations. *J. Am. Chem. Soc.* **2009**, *131*, 4702–4709.
- (33) Udommaneehanakit, T.; Rungrotmongkol, T.; Bren, U.; Frečer, V.; Stanislav, M. Dynamic behavior of avian influenza A virus neuraminidase subtype H5N1 in complex with oseltamivir, zanamivir, peramivir, and their phosphonate analogues. *J. Chem. Inf. Model.* **2009**, *49*, 2323–2332.
- (34) Park, J. W.; Jo, W. H. Computational design of novel, high-affinity neuraminidase inhibitors for H5N1 avian influenza virus. *Eur. J. Med. Chem.* **2010**, *45*, 536–541.
- (35) Wall, I. D.; Leach, A. R.; Salt, D. W.; Ford, M. G.; Essex, J. W. Binding constants of neuraminidase inhibitors: an investigation of the linear interaction energy method. *J. Med. Chem.* **1999**, *42*, 5142–5152.
- (36) Wang, T.; Wade, R. C. Comparative binding energy (COMBINE) analysis of influenza neuraminidase–inhibitor complexes. *J. Med. Chem.* **2001**, *44*, 961–971.
- (37) Masukawa, K. M.; Kollman, P. A.; Kuntz, I. D. Investigation of neuraminidase–substrate recognition using molecular dynamics and free energy calculations. *J. Med. Chem.* **2003**, *46*, 5628–5637.
- (38) Bonnet, P.; Bryce, R. A. Molecular dynamics and free energy analysis of neuraminidase–ligand interactions. *Protein Sci.* **2004**, *13*, 946–957.
- (39) Bonnet, P.; Bryce, R. A. Scoring binding affinity of multiple ligands using implicit solvent and a single molecular dynamics trajectory: application to influenza neuraminidase. *J. Mol. Graph. Model.* **2005**, *24*, 147–156.
- (40) Malaisree, M.; Rungrotmongkol, T.; Decha, P.; Intharathep, P.; Aruksakunwong, O.; Hannongbua, S. Understanding of known drug–target interactions in the catalytic pocket of neuraminidase subtype N1. *Proteins* **2008**, *71*, 1908–1918.
- (41) Li, Y.; Zhou, B.; Wang, R. Rational design of tamiflu derivatives targeting at the open conformation of neuraminidase subtype 1. *J. Mol. Graph. Model.* **2009**, *28*, 203–219.
- (42) Zhang, Q.; Yang, J.; Liang, K.; Feng, L.; Li, S.; Wan, J.; Xu, X.; Yang, G.; Liu, D.; Yang, S. Binding interaction analysis of the active site and its inhibitors for neuraminidase (N1 subtype) of human influenza virus by the integration of molecular docking, FMO calculation and 3D-QSAR CoMFA modeling. *J. Chem. Inf. Model.* **2008**, *48*, 1802–1812.
- (43) Yoshida, T.; Yamagishi, K.; Chuman, H. QSAR study of cyclic urea type HIV-1 PR inhibitors using ab initio MO calculation of their complex structures with HIV-1 PR. *QSAR Comb. Sci.* **2008**, *27*, 694–703.
- (44) Yoshida, T.; Fujita, T.; Chuman, H. Novel quantitative structure–activity studies of HIV-1 protease inhibitors of the cyclic urea type using descriptors derived from molecular dynamics and molecular orbital calculations. *Curr. Comput.-Aided Drug Des.* **2009**, *5*, 38–55.
- (45) Yoshida, T.; Munei, Y.; Hitaoka, S.; Chuman, H. Correlation analyses on binding affinity of substituted benzenesulfonamides with carbonic anhydrase using ab initio MO calculations on their complex structures. *J. Chem. Inf. Model.* **2010**, *50*, 850–860.
- (46) Kim, C. U.; Lew, W.; Williams, M. A.; Wu, H.; Zhang, L.; Chen, X.; Escarpe, P. A.; Mendel, D. B.; Laver, W. G.; Stevens, R. C. Structure–activity relationship studies of novel carbocyclic influenza neuraminidase inhibitors. *J. Med. Chem.* **1998**, *41*, 2451–2460.
- (47) Dimmock, N. J. Dependence of the activity of an influenza virus neuraminidase upon Ca^{2+} . *J. Gen. Virol.* **1971**, *13*, 481–483.
- (48) Carroll, S. M.; Paulson, J. C. Complete metal ion requirement of influenza virus N1 neuraminidases. *Arch. Virol.* **1982**, *71*, 273–277.
- (49) Chong, A. K. J.; Pegg, M. S.; von Itzstein, M. Influenza virus sialidase: effect of calcium on steady-state kinetic parameters. *Biochim. Biophys. Acta* **1991**, *1077*, 65–71.
- (50) Smith, B. J.; Huyton, T.; Joosten, R. P.; McKimm-Breschkin, J. L.; Zhang, J. G.; Luo, C. S.; Lou, M.-Z.; Labrou, N. E.; Garrett, T. P. J. Structure of a calcium-deficient form of influenza virus neuraminidase: implications for substrate binding. *Acta Crystallogr., Sect. D: Biol. Crystallogr.* **2006**, *62*, 947–952.
- (51) Collins, P. J.; Haire, L. F.; Lin, Y. P.; Liu, J.; Russell, R. J.; Walker, P. A.; Skehel, J. J.; Martin, S. R.; Hay, A. J.; Gamblin, S. J. Crystal structures of oseltamivir-resistant influenza virus neuraminidase mutants. *Nature* **2008**, *453*, 1258–1261.
- (52) Dolinsky, T. D.; Nielsen, J. E.; McCammon, J. A.; Baker, N. A. PDB2PQR: an automated pipeline for the setup, execution, and analysis of Poisson–Boltzmann electrostatics calculations. *Nucleic Acids Res.* **2004**, *32*, W665–W667.
- (53) Case, D. A.; Cheatham, T. E., III.; Darden, T.; Gohlke, H.; Luo, R.; Merz, K. M., Jr.; Onufriev, A.; Simmerling, C.; Wang, B.; Woods, R. J. The Amber biomolecular simulation programs. *J. Comput. Chem.* **2005**, *26*, 1668–1688.
- (54) Wang, J.; Cieplak, P.; Kollman, P. A. How well does a restrained electrostatic potential (RESP) model perform in calculating conformational energies of organic and biological molecules. *J. Comput. Chem.* **2000**, *21*, 1049–1074.
- (55) Wang, J.; Wolf, R. M.; Caldwell, J. W.; Kollman, P. A.; Case, D. A. Development and testing of a general Amber force field. *J. Comput. Chem.* **2004**, *25*, 1157–1174.
- (56) Bayly, C. I.; Cieplak, P.; Cornell, W. D.; Kollman, P. A. A well-behaved electrostatic potential based method using charge restraints for deriving atomic charges: the RESP model. *J. Phys. Chem.* **1993**, *97*, 10269–10280.
- (57) Frisch, M. J.; Trucks, G. W.; Schlegel, H. B.; Scuseria, G. E.; Robb, M. A.; Cheeseman, J. R.; Montgomery, J. A., Jr.; Vreven, T.; Kudin, K. N.; Burant, J. C.; Millam, J. M.; Iyengar, S. S.; Tomasi, J.; Barone, V.; Mennucci, B.; Cossi, M.; Scalmani, G.; Rega, N.; Petersson, G. A.; Nakatsuji, H.; Hada, M.; Ehara, M.; Toyota, K.; Fukuda, R.; Hasegawa, J.; Ishida, M.; Nakajima, T.; Honda, Y.; Kitao, O.; Nakai, H.; Klene, M.; Li, X.; Knox, J. E.; Hratchian, H. P.; Cross, J. B.; Bakken, V.; Adamo, C.; Jaramillo, J.; Gomperts, R.; Stratmann, R. E.; Yazyev, O.; Austin, A. J.; Cammi, R.; Pomelli, C.; Ochterski, J. W.; Ayala, P. Y.; Morokuma, K.; Voth, G. A.; Salvador, P.; Dannenberg, J. J.; Zakrzewski, V. G.; Dapprich, S.; Daniels, A. D.; Strain, M. C.; Farkas, O.; Malick, D. K.; Rabuck, A. D.; Raghavachari, K.; Foresman, J. B.; Ortiz, J. V.; Cui, Q.; Baboul, A. G.; Clifford, S.; Cioslowski, J.; Stefanov, B. B.; Liu, G.; Liashenko, A.; Piskorz, P.; Komaromi, I.; Martin, R. L.; Fox, D. J.; Keith, T.; Al-Laham, M. A.; Peng, C. Y.; Nanayakkara, A.; Challacombe, M.; Gill, P. M. W.; Johnson, B.; Chen, W.; Wong, M. W.; Gonzalez, C.; Pople, J. A. *Gaussian 03, Revision C.02*; Gaussian, Inc.: Wallingford, CT, 2004.
- (58) Bayly, C. I.; Cieplak, P.; Cornell, W. D.; Kollman, P. A. A well-behaved electrostatic potential based method using charge restraints for deriving atomic charges: the RESP model. *J. Phys. Chem.* **1993**, *97*, 10269–10280.
- (59) Cornell, W. D.; Cieplak, P.; Bayly, C. I.; Kollman, P. A. Application of RESP charges to calculate conformational energies, hydrogen bond energies, and free energies of solvation. *J. Am. Chem. Soc.* **1993**, *115*, 9620–9631.
- (60) Bren, U.; Hodošek, M.; Koller, J. Development and validation of empirical force field parameters for netropsin. *J. Chem. Inf. Model.* **2005**, *45*, 1546–1552.
- (61) Berendsen, H. J. C.; Postma, J. P. M.; van Gunsteren, W. F.; DiNola, A.; Haak, J. R. Molecular dynamics with coupling to an external bath. *J. Chem. Phys.* **1984**, *81*, 3684–3690.
- (62) Ryckaert, J.-P.; Ciccotti, G.; Berendsen, H. J. C. Numerical integration of the cartesian equations of motion of a system with constraints: molecular dynamics of *n*-alkanes. *J. Comput. Phys.* **1977**, *23*, 327–341.
- (63) Darden, T. A.; York, D. M.; Pedersen, L. G. Particle mesh Ewald: an $N \cdot \log(N)$ method for Ewald sums in large systems. *J. Chem. Phys.* **1993**, *98*, 10089–10092.
- (64) Ladbury, J. E. Just add water! the effect of water on the specificity of protein–ligand binding sites and its potential application to drug design. *Chem. Biol.* **1996**, *3*, 973–980.
- (65) Swaminathan, C. P.; Suroli, N.; Suroli, A. Role of water in the specific binding of mannose and mannooligosaccharides to concanavalin A. *J. Am. Chem. Soc.* **1998**, *120*, 5153–5159.
- (66) Clarke, C.; Woods, R. J.; Gluska, J.; Cooper, A.; Nutley, M. A.; Boons, G.-J. Involvement of water in carbohydrate–protein binding. *J. Am. Chem. Soc.* **2001**, *123*, 12238–12247.
- (67) Fukuzawa, K.; Kitaura, K.; Uebayasi, M.; Nakata, K.; Kaminuma, T.; Nakano, T. Ab initio quantum mechanical study of the binding energies of human estrogen receptor α with its ligands: an application of fragment molecular orbital method. *J. Comput. Chem.* **2005**, *26*, 1–10.
- (68) Yoshida, T.; Lepp, Z.; Kadota, Y.; Satoh, Y.; Itoh, K.; Chuman, H. Comparative analysis of binding energy of chymotrypsin with human cathepsin A and its homologous proteins by molecular orbital calculation. *J. Chem. Inf. Model.* **2006**, *46*, 2093–2103.
- (69) Kitaura, K.; Ikeo, E.; Asada, T.; Nakano, T.; Uebayasi, M. Fragment molecular orbital method: an approximate computational method for large molecules. *Chem. Phys. Lett.* **1999**, *313*, 701–706.
- (70) Iwata, T.; Fukuzawa, K.; Nakajima, K.; Aida-Hyugaji, S.; Mochizuki, Y.; Watanabe, H.; Tanaka, S. Theoretical analysis of binding specificity of influenza viral hemagglutinin to avian and human receptors based on the fragment molecular orbital method. *Comput. Biol. Chem.* **2008**, *32*, 198–211.

- (71) Nakano, T.; Mochizuki, Y.; Kato, A.; Fukuzawa, K.; Ishikawa, T.; Amari, S.; Kurisaki, I.; Tanaka, S. Developments of FMO methodology and graphical user interface in ABINIT-MP. In *The Fragment Molecular Orbital Method: Practical Applications to Large Molecular Systems*; Fedorov, D. G., Kitaura, K., Eds.; CRC Press: Boca Raton, FL, 2009; pp 37–59.
- (72) Mochizuki, Y.; Nakano, T.; Koikegami, S.; Tanimori, S.; Abe, Y.; Nagashima, U.; Kitaura, K. A parallelized integral-direct second-order Møller-Plesset perturbation theory method with a fragment molecular orbital scheme. *Theor. Chem. Acc.* **2004**, *112*, 442–452.
- (73) Fedorov, D. G.; Kitaura, K. Theoretical development of the fragment molecular orbital (FMO) method. In *Modern Methods for Theoretical Physical Chemistry of Biopolymers*; Starikov, E. B., Lewis, J. P., Tanaka, S., Eds.; Elsevier: Amsterdam, 2006; pp 3–38.
- (74) Meyer, E. A.; Castellano, R. K.; Diederich, F. Interactions with aromatic rings in chemical and biological recognition. *Angew. Chem., Int. Ed.* **2003**, *42*, 1210–1250.
- (75) Ishikawa, T.; Mochizuki, Y.; Amari, S.; Nakano, T.; Tokiwa, H.; Tanaka, S.; Tanaka, K. Fragment interaction analysis based on local MP2. *Theor. Chem. Acc.* **2007**, *118*, 937–945.
- (76) He, X.; Fusti-Molnar, L.; Cui, G.; Merz, K. M., Jr. Importance of dispersion and electron correlation in ab initio protein folding. *J. Phys. Chem. B* **2009**, *113*, 5290–5300.
- (77) Varghese, J. N.; Smith, P. W.; Sollis, S. L.; Blick, T. J.; Sahasrabudhe, A.; McKimm-Breschkin, J. L.; Colman, P. M. Drug design against a shifting target: a structural basis for resistance to inhibitors in a variant of influenza virus neuraminidase. *Structure* **1998**, *6*, 735–746.
- (78) Smith, B. J.; McKimm-Breshkin, J. L.; McDonald, M.; Fernley, R. T.; Varghese, J. N.; Colman, P. M. Structural studies of the resistance of influenza virus neuraminidase to inhibitors. *J. Med. Chem.* **2002**, *45*, 2207–2212.
- (79) Lee, B.; Richards, F. M. The interpretation of protein structures: estimation of static accessibility. *J. Mol. Biol.* **1971**, *55*, 379–400.
- (80) Chothia, C. Hydrophobic bonding and accessible surface area in proteins. *Nature* **1974**, *248*, 338–339.
- (81) Chuman, H.; Mori, A.; Tanaka, H.; Yamagami, C.; Fujita, T. Analyses of the partition coefficient, log P, using ab initio MO parameter and accessible surface area of solute molecules. *J. Pharm. Sci.* **2004**, *93*, 2681–2697.
- (82) Scott, A. D.; Phillips, C.; Alex, A.; Flocco, M.; Bent, A.; Randall, A.; O'Brien, R.; Damian, L.; Jones, L. H. Thermodynamic optimization in drug discovery: a case study using carbonic anhydrase inhibitors. *Chem. Med. Chem.* **2009**, *4*, 1985–1989.
- (83) Frederick, K. K.; Marlow, M. S.; Valentine, K. G.; Wand, A. J. Conformational entropy in molecular recognition by proteins. *Nature* **2007**, *448*, 325–329.
- (84) Gloster, T. M.; Meloncelli, P.; Stick, R. V.; Zechel, D.; Vasella, A.; Davies, G. J. Glycosidase inhibition: an assessment of the binding of 18 putative transition-state mimics. *J. Am. Chem. Soc.* **2007**, *129*, 2345–2354.
- (85) Gloster, T. M.; Davies, G. J. Glycosidase inhibition: assessing mimicry of the transition state. *Org. Biomol. Chem.* **2010**, *8*, 305–320.
- (86) Wen, W.-H.; Wang, S.-Y.; Tsai, K.-C.; Cheng, Y.-S. E.; Yang, A.-S.; Fang, J.-M.; Wong, C.-H. Analogs of zanamivir with modified C4-substituents as the inhibitors against the group-1 neuraminidases of influenza viruses. *Bioorg. Med. Chem.* **2010**, *18*, 4074–4084.
- (87) Perdih, A.; Bren, U.; Solmajer, T. Binding free energy calculations of *N*-sulphonyl-glutamic acid inhibitors of MurD ligase. *J. Mol. Model.* **2009**, *15*, 983–996.
- (88) Sham, Y. Y.; Chu, Z. T.; Tao, H.; Warshel, A. Examining methods for calculations of binding free energies: LRA, LIE, PDL-D-LRA, and PDL-D/S-LRA calculations of ligands binding to an HIV protease. *Proteins* **2000**, *39*, 393–407.
- (89) Bren, U.; Lah, J.; Bren, M.; Martinek, V.; Florián, J. DNA duplex stability: the role of preorganized electrostatics. *J. Phys. Chem. B* **2010**, *114*, 2876–2885.
- (90) Bren, U.; Martinek, V.; Florián, J. Decomposition of the solvation free energies of deoxyribonucleoside triphosphates using the free energy perturbation method. *J. Phys. Chem. B* **2006**, *110*, 12782–12788.
- (91) Bren, M.; Florián, J.; Mavri, J.; Bren, U. Do all pieces make a whole? Thiele cumulants and the free energy decomposition. *Theor. Chem. Acc.* **2007**, *117*, 535–540.

CI100225B